applied sciences

MDPI

Article

Slope Stability Analysis of Open-Pit Mine Considering Weathering Effects

Wei Liu [1], Gang Sheng [1], Xin Kang [1], Min Yang [2], Danqi Li [3] and Saisai Wu [2,*]

[1] Ankang Branch of Shaanxi Provincial Land Engineering Construction Group Co., Ltd., Ankang 725000, China
[2] School of Resources Engineering, Shanxi Key Laboratory of Geotechnical and Underground Space Engineering, XAUAT, Xi'an 710055, China
[3] Minerals, Energy and Chemical Engineering, Curtin University, Kalgoorlie, WA 6430, Australia; danqi.li@curtin.edu.au
* Correspondence: saisai.wu@xauat.edu.cn

Abstract: Weathering processes gradually alter the physical and mechanical attributes of slope materials, weakening the structural integrity and stability of slopes. This paper presents an in-depth analysis of slope stability in an open-pit mine, emphasizing the pivotal role of weathering effects in determining slope stability. To accurately capture the impact of weathering on slope stability, a comprehensive analysis model was developed, incorporating field observations, laboratory testing, and numerical simulations. The effects of weathering on the mechanical properties of black shale were studied through extensive laboratory tests. The uniaxial compressive strength, shear strength, and modulus of elasticity significantly decreased with increasing weathering, indicating a heightened vulnerability to slope failure. The correlation function between mechanical parameters and weathering time was obtained, providing the basis for evaluating the stability of mine slopes. It was found that more severe weathering conditions were strongly correlated with elevated risks of slope failure, including landslides and collapses. Based on these findings, practical recommendations are provided for slope reinforcement and management strategies, aimed at mitigating slope failure risks and ensuring the safe and efficient operation of the mine. By incorporating weathering effects into slope stability analysis, mine operators can make informed decisions that account for the dynamic nature of slope materials and their susceptibility to weathering, thereby improving overall mine performance and safety.

Keywords: slope stability; weathering; black shale; mechanical properties

Citation: Liu, W.; Sheng, G.; Kang, X.; Yang, M.; Li, D.; Wu, S. Slope Stability Analysis of Open-Pit Mine Considering Weathering Effects. *Appl. Sci.* **2024**, *14*, 8449. https://doi.org/10.3390/app14188449

Academic Editor: Tiago Miranda

Received: 29 July 2024
Revised: 12 September 2024
Accepted: 16 September 2024
Published: 19 September 2024

1. Introduction

Slope stability analysis is a pivotal aspect of mine planning and operations in open-pit mines, as it directly impacts the safety of mine workers and the efficiency of mining activities [1–3]. Over the years, numerous studies have been conducted to assess slope stability. With the advancing technology in open-pit mining, the scale and depth of excavations are constantly increasing. Slope stability is a crucial aspect of civil engineering and geotechnical studies. The following are the most influential parameters in slope stability: soil properties, geological structure, slope geometry, groundwater conditions, and external loads [4]. As the depth of mining increases, slope heights are also escalating annually, resulting in concave or deeply concave mining fields. In open-pit mines, every marginal increase in slope angle can significantly augment the stripping volume, emphasizing the importance of optimizing slope design and accurately evaluating slope stability [5,6]. Therefore, a comprehensive approach to slope stability analysis, considering various factors such as geological conditions and weathering effects is essential for ensuring the safety and sustainability of mining operations.

Slope stability is often influenced by a range of geological and environmental factors, with weathering effects being particularly significant contributors [7–10]. Rocks vary

in composition and structure, leading to differences in stress–strain relationships and deformation characteristics. These properties are further influenced by factors such as temperature and humidity, which are integral parts of the weathering process [11–15]. Rock weathering is a natural process that involves the gradual breakdown and alteration of rocks due to their interactions with the environment over time [16–20]. This ongoing process leads to intricate changes in the petrographical, mineralogical, microstructural, and geomechanical properties of rocks. Typically, weathering reduces the strength of rocks by enhancing the deformability and degradation. Furthermore, weathering alters the mineral composition of rocks, causing certain minerals to undergo dissolution, oxidation, or hydrolysis through chemical reactions. These chemical alterations result in changes in the physical and mechanical properties, further compromising the tensile strength of rock and increasing its vulnerability to failure [21]. Given the adverse impact of weathering on strength and deformational characteristics of rocks, a thorough evaluation of the physical–mechanical behavior of rocks under weathering conditions is crucial in the context of underground mines [22,23]. Previous investigations into the geotechnical state of railway tunnels have revealed that weathering can pose significant challenges, leading to substantial economic losses [24].

Numerous studies have been conducted to evaluate the effects of weathering on the mechanical properties of granitoid rocks. Heidari and Momeni [25] observed a decrease in the elastic modulus of granodiorite as weathering time increased. Leveraging the correlation between weathering grades and changes in mechanical and petrographic properties, Momeni and Khanlari established a weathering classification system for granitoid rocks. Abad and Tugrul [26] delved into the characteristics of granitic rock masses across various weathering zones in tropical environments. Additionally, researchers have discovered that weathering reduces the elastic modulus of rocks by modifying their mineralogical characteristics. Specifically, for calcareous rocks, the elastic modulus has been shown to exhibit a negative exponential relationship with calcite content.

In open-pit mines, weathering can significantly reduce the strength and stability of slope materials, posing potential safety hazards [27–32]. Despite the crucial role of weathering effects in determining slope stability, many traditional analysis methods overlook or oversimplify these factors [33–38]. This approach can lead to inaccurate predictions of slope stability and potentially underestimate the risks of slope failure. Therefore, it is imperative to incorporate weathering effects into slope stability assessments to ensure the safe and efficient operation of mines. Additionally, a thorough understanding of the mechanical properties of rocks at a given time and location is crucial for studying related geotechnical engineering. The process of ore mining itself involves studying the mechanical properties of rocks. Gaining a comprehensive understanding of the physical and mechanical properties of surrounding rocks, particularly under the influence of weathering, holds significant theoretical and practical value. It is essential for ensuring the safe mining of open-pit mines and optimizing mining boundaries.

Although weathering effects play a crucial role in determining slope stability, few researchers have investigated the effects of weathering and the traditional analysis methods either overlook these factors or oversimplify them. In this study, a comprehensive analysis of slope stability in open-pit mines, taking into account the influence of weathering effects, was conducted. Laboratory tests were performed to investigate the impact of weathering on the mechanical properties of black-shale specimens. Numerical simulations were employed to evaluate slope stability and determine safety factors under various weathering conditions. By incorporating weathering effects into slope stability analysis, this study aimed to provide a more accurate and reliable assessment of slope stability in open-pit mines. The findings of this research could significantly contribute to enhancing mine safety, mitigating slope failure risks, and optimizing mine planning and operations.

2. Laboratory Tests of Weathering Effects

2.1. Testing Specimens

The engineering background of this study was one of the phosphate mines located in Yunnan Province, China. The predominant rock type surrounding the ore body in this mine is black shale. Given the low strength and rapid weathering characteristics of black shale in the mining area, the stability of the slopes, as well as the optimization of slope angles and boundaries, pose significant concerns. To address the concerns, black-shale samples collected from the mining areas were utilized as specimens to determine their fundamental mechanical properties under weathering effects. This particular phosphate mine was located at the northern edge of the Yunnan–Guizhou Plateau, where the terrain is complex with intense cutting and well-developed valleys, belonging to the deeply incised karst highland mountain landforms. The topography of the mining area is steep, with ore outcrops at altitudes ranging from 2600 to 3000 m. These topographical conditions have a significant impact on the preservation and enrichment depth of weathering products. The rock specimens were drilled perpendicular to the bedding direction at the depth of 600 m and processed into standard cylindrical specimens, which was in accordance with the rock mechanics test specification recommended by the International Society for Rock Mechanics (ISRM) [39]. Weathering may alter the mineral composition and physical properties of rocks, as well as their mechanical properties, but only the mechanical properties were focused on in this study. For the uniaxial compression test, the specimens had a diameter of 50 mm and a height-to-diameter ratio of 2. For the direct shear mechanical test, the height-to-diameter ratio was set to 1, while for the Brazilian splitting test it was 0.5. The specimens used for each test are shown in Figure 1.

Figure 1. Examples of the specimens: (**a**) Brazilian splitting test, (**b**) uniaxial compression test, and (**c**) direct shear test.

2.2. Experimental Methodologies

A comprehensive suite of tests, including uniaxial compressive strength tests, direct shear tests, and Brazilian splitting tests, were conducted on the specimens (Figure 2). For the uniaxial compressive strength tests the specimen was placed between the platens of a compressive testing machine. A gradually increasing compressive load at 0.5 MPa/s was applied to the specimen at a controlled rate. For direct shear tests, the specimen was placed between the upper and lower shear boxes. A predetermined normal load was applied to the specimen to simulate the in situ stress conditions. A gradually increasing horizontal load at 0.1 MPa/s was applied to cause shear deformation. For the Brazilian splitting tests, the specimen was placed between two loading platens. A compressive load at 0.5 MPa/s was applied along the diameter of the specimen. Prior to testing, the specimens were carefully placed in the actual mining environment to undergo natural weathering. The specimens were placed in the areas near the slope edge where significant diurnal temperature range co-occurs during day and night, which is a prominent feature of the plateau climate. To understand the evolution of physical and mechanical parameters during weathering, the specimens were periodically retrieved, and examined for relevant physical and mechanical parameters. The testing programs are outlined in Table 1. A total of 15 Brazilian splitting tests, 15 uniaxial compression tests, and 15 direct shear tests were conducted. During the tests, since the weathering process occurred in the actual mining environment, the temperature as well as the precipitation were different each day. It was recorded that the

maximum surface temperature reached 75.2 °C, while the minimum surface temperature was 16.4 °C, resulting in a temperature difference of 55.8 °C. The large diurnal temperature variation not only affected the physical properties of rocks, such as causing micro-cracks on the surface of rocks, but also promoted the freeze–thaw weathering process of rocks. When the temperature dropped at night, moisture on the surface of rocks easily condensed into frost or ice, exerting a freezing force on the rocks, thereby accelerating the weathering process. The area also has abundant precipitation, and weathering was even more intense. It was recorded that during the 28 days of weathering, there were 9 days of rain.

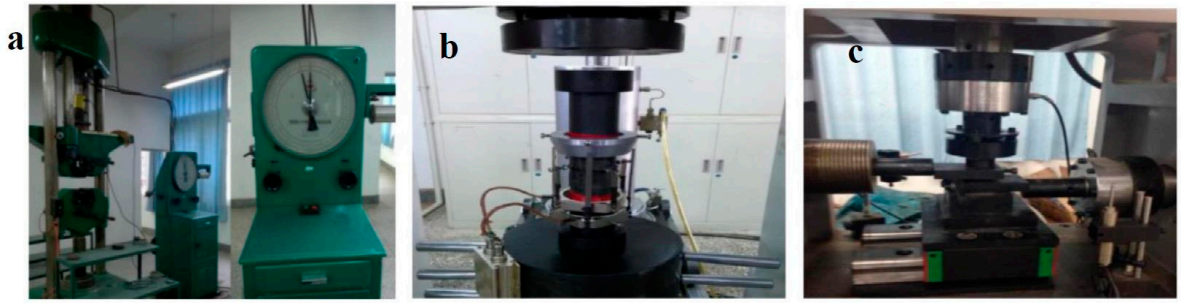

Figure 2. Testing equipment: (**a**) uniaxial compressive strength test, (**b**) direct shear test, and (**c**) Brazilian splitting test.

Table 1. The design of the experimental programs.

ID	Weathering (Days)	Number of Specimens		
		Brazilian Split Tests	Uniaxial Compression Tests	Direct Shear Tests
1	0	3	3	3
2	7	3	3	3
3	14	3	3	3
4	21	3	3	3
5	28	3	3	3

2.3. Mechanical Properties Test Results

The weathering effects exerted a profound influence on the experimental outcomes of the Brazilian splitting test. The failed specimens in the Brazilian splitting tests, uniaxial compression tests, and direct shear tests are displayed in Figure 3. As detailed in Table 2, the average tensile strengths of black shale decreased gradually with the increase in weathering time. The integrity of the rocks was compromised by weathering, leading to an increase in microcracks and porosity within the rock matrix. This, in turn, diminished the overall strength of the rock. In the case of unweathered rocks, the Brazilian splitting test typically produced relatively smooth and flat fracture surfaces. However, weathered rocks exhibited irregular fracture surfaces due to the presence of internal microcracks and pores, resulting in multiple fracture planes. This phenomenon contributed to the increased dispersion of test results.

Table 2. The average tensile strengths of black shale at different weathering times.

Weathering (Days)	Specimen		Tensile Strength
	Diameter (mm)	Height (mm)	
0	47.08	23.6	9.82
7	46.94	24.42	6.91
14	47.36	24.12	5.09
21	47.20	24.02	4.02
28	47.26	23.96	2.98

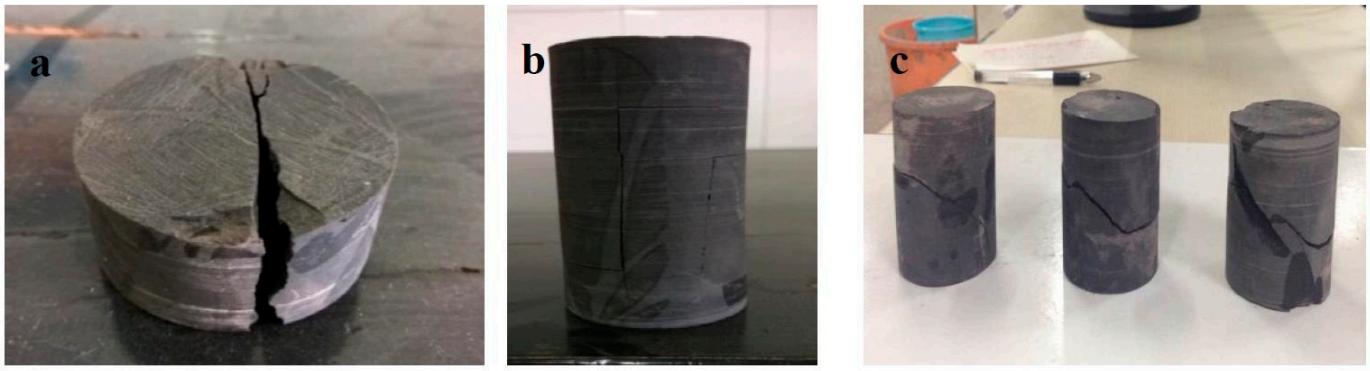

Figure 3. The failed specimens: (**a**) Brazilian splitting test, (**b**) uniaxial compression test, and (**c**) direct shear test.

The uniaxial compression tests revealed that weathering significantly affected the compression properties of the rocks (Table 3). As weathering progressed, the uniaxial compressive strength and elastic modulus of black shale gradually decreased, while the Poisson's ratio gradually increased. The decrease in elastic modulus indicated that the rock became more susceptible to deformation under external forces. This is attributed to the gradual development of transverse and longitudinal cracks within the rock during the weathering process. These cracks weaken the structural integrity of the rock, leading to a reduction in its compressive strength and stiffness. The longitudinal cracks directly contribute to the decrease in uniaxial compressive strength of the specimen, while the development of transverse cracks accelerates radial deformation during the loading process. Consequently, the Poisson's ratio gradually increases with the increase in weathering time. This decline in strength can be attributed to the breakdown of mineral grains and the formation of microcracks and pores within the rock matrix. Furthermore, weathering enhances the deformability of rocks. Rock specimens with higher degrees of weathering exhibit greater strain under compressive loads compared with their less weathered counterparts. This enhanced deformability is primarily due to the softening of the rock matrix and the development of microcracks and pores.

Table 3. The uniaxial compression mechanical parameters of black shale at different weathering times.

Weathering (Days)	Specimen		Uniaxial Compression Strength (MPa)	Elastic Modulus (GPa)	Poisson's Ratio
	Diameter (mm)	Height (mm)			
0	47.22	95.44	66.48	13.29	0.160
7	47.18	95.80	39.51	4.70	0.295
14	47.26	96.26	24.25	4.34	0.339
21	47.04	94.46	15.29	3.92	0.379
28	47.12	95.08	10.09	3.55	0.408

The mechanical properties of black shale obtained from direct shear tests at various weathering times are displayed in Figure 4. The test results demonstrate significant decreases in shear strength for the weathered rocks. During the direct shear tests, a linear correlation was observed between the deformation and the applied load, as summarized in Table 4. This linearity suggests that the rocks exhibited elastic behavior until they reached the point of failure. Based on this linear relationship, the cohesion and internal friction angle of black shale were calculated. Generally, as the weathering time increased, the cohesion and internal friction angle of the black shale tended to decrease gradually. This decrease in shear strength can be attributed to the weakening of the rock matrix due to weathering processes. Weathering leads to the breakdown of mineral grains, resulting in the formation of cracks and pores within the rock structure. The cracks and pores reduce

the effective contact area between the grains, thereby decreasing the shear strength of the rock.

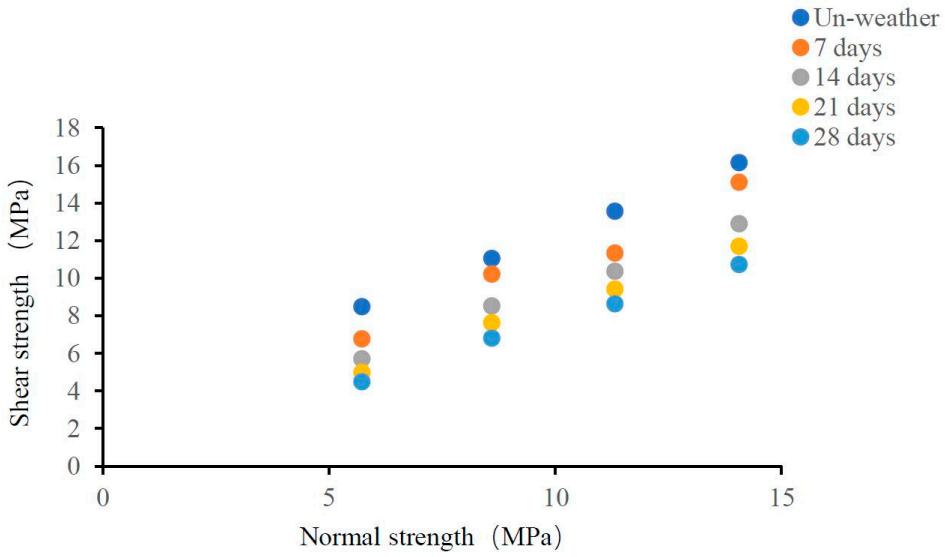

Figure 4. The direct shear testing parameters at different weathering times.

Table 4. Cohesion and internal friction angle at different weathering times.

Weathering (Days)	Fitting Results	Correlation Coefficient (R2)	Cohesion	Internal Friction Angle
0	y = 0.9086x + 3.2702	0.9999	3.28	42.22
7	y = 0.9298x + 1.6042	0.9611	1.60	42.92
14	y = 0.8398x + 1.0663	0.9941	1.07	40.02
21	y = 0.7849x + 0.6717	0.9946	0.67	38.10
28	y = 0.7368x + 0.3809	0.9977	0.38	36.41

A comprehensive set of physical and mechanical parameters was obtained through laboratory tests, which included uniaxial compressive strength, elastic modulus, Poisson's ratio, uniaxial tensile strength, cohesion, and internal friction angles, as detailed in Tables 5 and 6. Additionally, the determination coefficients for each correlation function are also provided. The uniaxial tensile strength, uniaxial compression strength, and cohesion of the rock specimens exhibited a negative exponential relationship with weathering time. This indicates that as the weathering time increased, these mechanical properties decreased The modulus of elasticity demonstrated a negative quadratic relationship with weathering time, suggesting a decrease in stiffness over time. Conversely, the Poisson's ratio exhibited a positive quadratic relationship with weathering time, indicating an increase in lateral deformation relative to axial deformation.

Table 5. Mechanical properties of black shale obtained from laboratory tests.

Weathering (Days)	Uniaxial Tensile Strength (MPa)	Uniaxial Compression Strength (MPa)	Elastic Modulus (GPa)	Poisson's Ratio	Internal Friction Angle	Cohesion (MPa)
0	9.82	66.48	13.29	0.160	42.22	3.28
7	6.91	39.51	4.70	0.295	42.92	1.60
14	5.09	24.25	4.34	0.339	40.02	1.07
21	4.02	15.29	3.92	0.379	38.10	0.67
28	2.98	10.09	3.55	0.408	36.41	0.38

Table 6. The correlation function between mechanical parameters and weathering time.

Parameters	Type of Function	Fitting Formula	Correlation Coefficient (R2)
Uniaxial tensile strength	Exponential	$y = 9.4964 \times 10^{-0.042}x$	0.9957
Uniaxial compression strength	Exponential	$y = 64.337 \times 10^{-0.067}x$	0.9982
Elastic modulus	Quadratic	$y = 0.0157 \times 2 - 0.7738x + 13.079$	0.9939
Poisson's ratio	Quadratic	$y = -0.0003 \times 2 + 0.0171x + 0.1693$	0.9797
Cohesion	Exponential	$y = 3.0276 \times 10^{-0.074}x$	0.9916

The correlation functions derived between weathering time and mechanical properties offer profound insights into deleterious effects of weathering on rocks. As the degree of weathering intensified, the elastic modulus of the rock diminished, indicating a heightened susceptibility to deformation under external forces. Weathering compromises the structural integrity of rocks, leading to the formation of microcracks and voids within the rock matrix. These microstructural defects not only weaken the tensile strength of the rock but also serve as stress concentration points, predisposing the rock to failure at lower stress levels. Weathering weakens the structural planes within rocks, leading to a decrease in cohesion and internal friction angles. This reduction in the strength of structural planes contributes to the overall decline in the rock's tensile strength, making it more susceptible to failure under tensile loads. The observed reduction in strength, augmentation of deformability, and enhancement of permeability of weathered rocks carry profound implications for a range of engineering applications. Consequently, it is imperative to meticulously consider the impact of weathering during the design and analysis of rock engineering projects. It is worth noting that weathering is a highly intricate process influenced by numerous factors. Therefore, when conducting experiments and analyzing data, it is essential to comprehensively account for various factors to ensure the accuracy and reliability of the findings.

3. Numerical Simulation of Slope Stability Analysis

3.1. Numerical Simulation Methodologies

To incorporate the influences of weathering into slope stability analysis, Fast Lagrangian Analysis of Continua (FLAC3D, Version 5.00) was utilized, which was developed by the Itasca Company, USA. FLAC3D is a simulation and calculation software that specializes in simulating and analyzing the plastic flow behavior of three-dimensional structures composed of soil, rock, and other materials. The software can accurately simulate the plastic failure and flow characteristics of materials, making it particularly suitable for simulating large deformation problems and nonlinear stress–strain relationships. The physical and mechanical parameters of the rock mass and various rock types within the mining area were obtained through site investigation. The method for obtaining the overburden thickness and mechanical properties of the open-pit mine was through drilling measurement technology. The cores extracted from the boreholes were analyzed for their physical and mechanical properties. A total of 12 boreholes were drilled, with the obtained results displayed in Table 7.

Table 7. The physical and mechanical parameters of other rock types in mining areas.

Rock Properties	Uniaxial Compressive Strength/MPa	Elastic Modulus/GPa	Tensile Strength/MPa	Poisson's Ratio	Cohesive Strength/MPa	Internal Friction Angle/°
Phosphate ore layer	50.27	15.80	5.57	0.29	12.78	41.30
Light gray dolomite	48.13	12.05	3.68	0.34	7.48	31.30
Dark gray dolomite	59.10	16.26	6.18	0.28	13.05	47.23

During the modeling process, a reasonable degree of simplification was applied to the geological prototype of the slope to ensure computational efficiency and accuracy. For the boundary conditions, the exposed surface of the slope was designated as the free boundary, while the bottom and both sides were constrained with normal displacement boundaries. The initial stress field was primarily determined by considering the self-weight stress of the rock mass. Initially, the stress field of the model was set to achieve equilibrium, reflecting the undisturbed geological conditions. The constitutive model and material division within the mining areas are clearly depicted in Figure 5. The model was configured with the X-direction aligned with the slope inclination and extending 1000 m in length, while the Y-direction represented the vertical direction with a height of 500 m. Taking into account the geological environment conditions, topography, and lithology of the open-pit slope in the mining areas, two models were specifically designed with final slope angles of 45° and 47°. These models were employed to simulate the gradual development of the open-pit slope. To delve deeper into consequences of weathering on slope stability, the mechanical parameters of black shale were adjusted to reflect various degrees of weathering, as outlined in Table 5. By incorporating the weathered properties, the model was able to simulate the altered behavior of the slope under the influence of weathering.

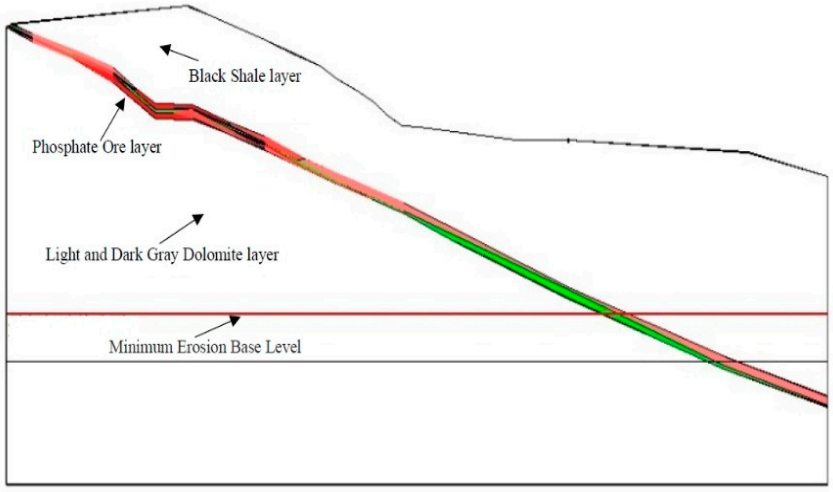

Figure 5. Constitutive model and material division in the mining areas.

3.2. Weathering Assessment Results

The computational model established for slope stability analysis was tailored to reflect the specific geological conditions. The model dimensions were approximately 900 m × 360 m, and it was discretized into 170 × 66 grids. In the real mining operations, the open-pit slope is excavated down to the current level of 2080 m, resulting in a slope height of 50 m. Subsequently, the slope is further excavated to the next stage, increasing its height to 90 m. This process continues, with the slope advancing to subsequent stages and ultimately reaching a height of 120 m. Therefore, to assess the slope stability under varying conditions, simulations and calculations were conducted using slope heights of 50 m, 90 m, and 120 m. These calculations were performed for slope angles of both 45° and 47°, taking into account the mechanical properties of the rock mass at different weathering degrees. For each step height, a detailed analysis was conducted to evaluate the slope stability at both slope angles, incorporating the varying mechanical parameters associated with different weathering degrees. As an illustrative example, the calculated results for a slope height of 50 m, slope angles of 45° and 47°, and a weathering time of 28 days are presented in Figures 6 and 7.

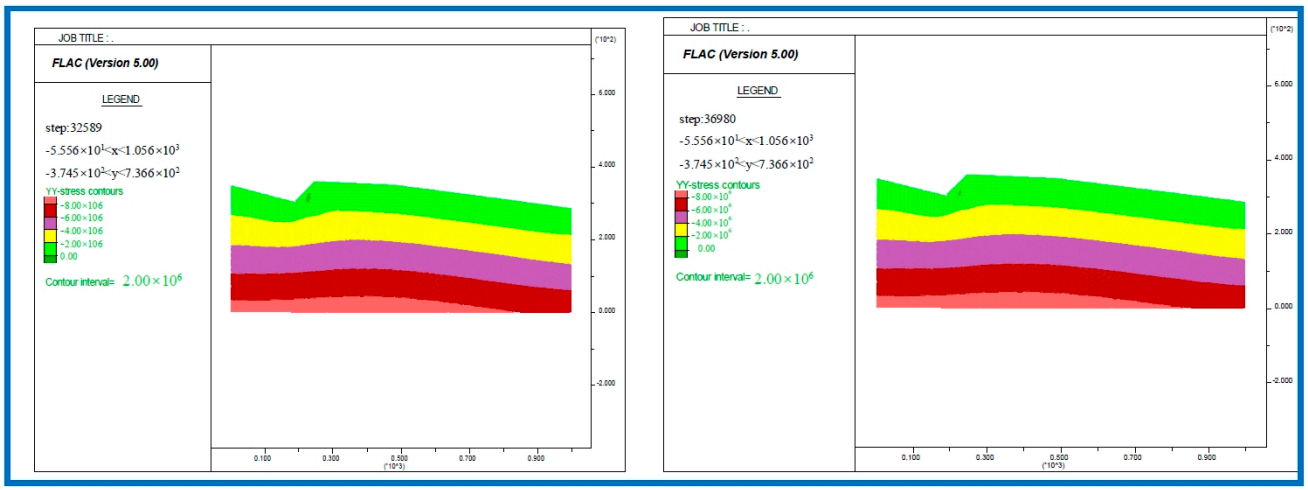

a: Vertical stress distribution, Unweathered (left), at weathering time of 28 days (right)

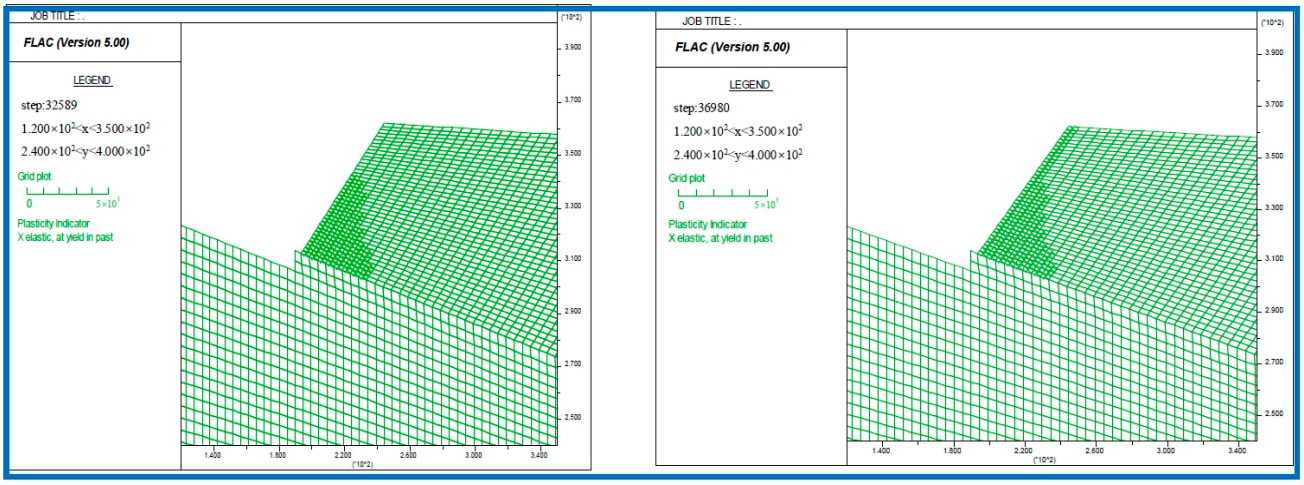

b: Plastic-zone distribution, Unweathered (left), at weathering time of 28 days (right)

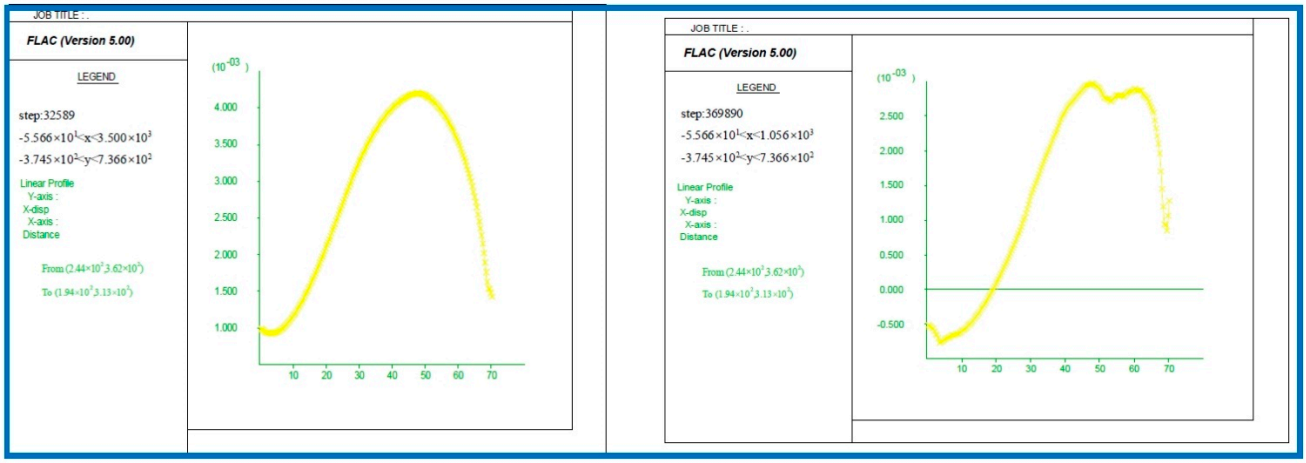

c: Horizontal-displacement distribution curve of slope surface, Unweathered (left), at weathering time of 28 days (right)

Figure 6. Calculated results for slope height of 50 m at angle of 45°.

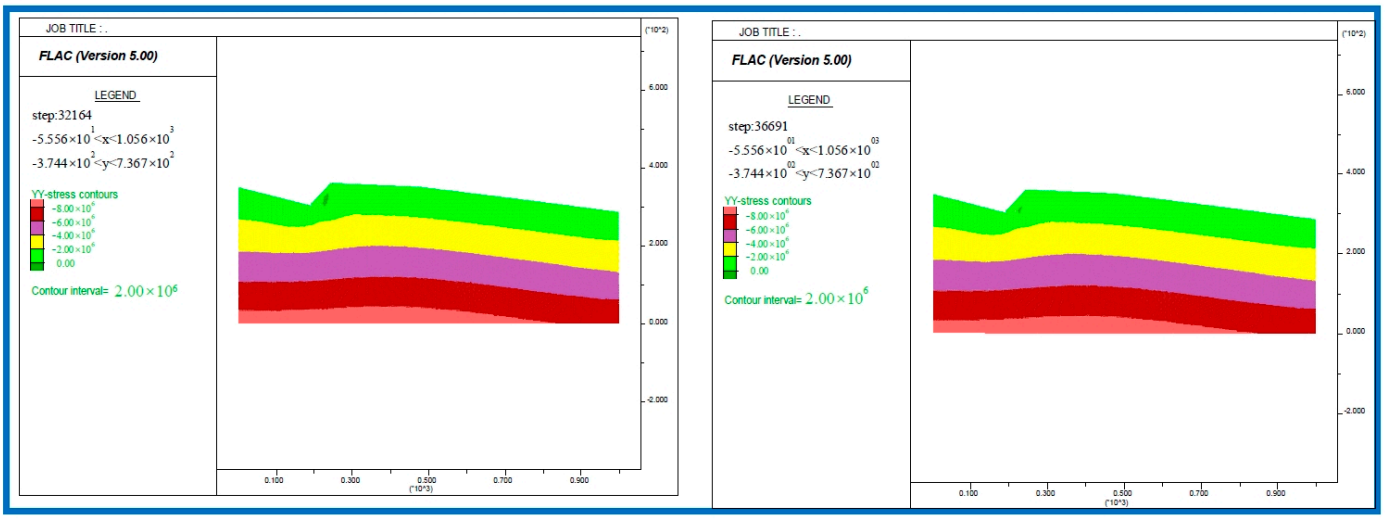

a: Vertical stress distribution, Unweathered (left), at weathering time of 28 days (right)

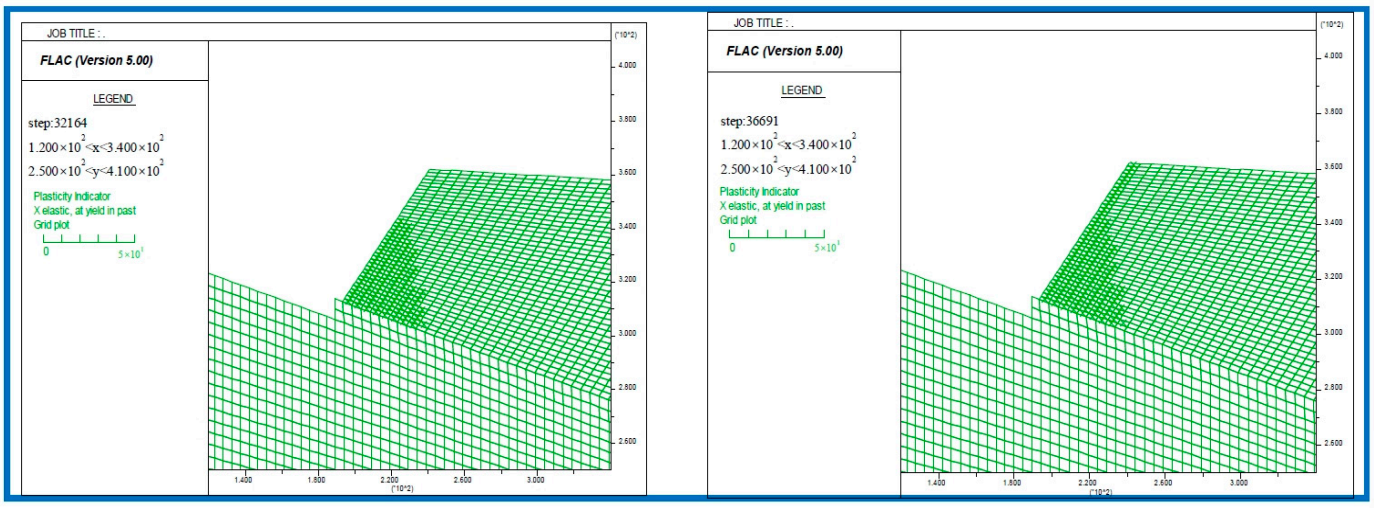

b: Plastic-zone distribution, Unweathered (left), at weathering time of 28 days (right)

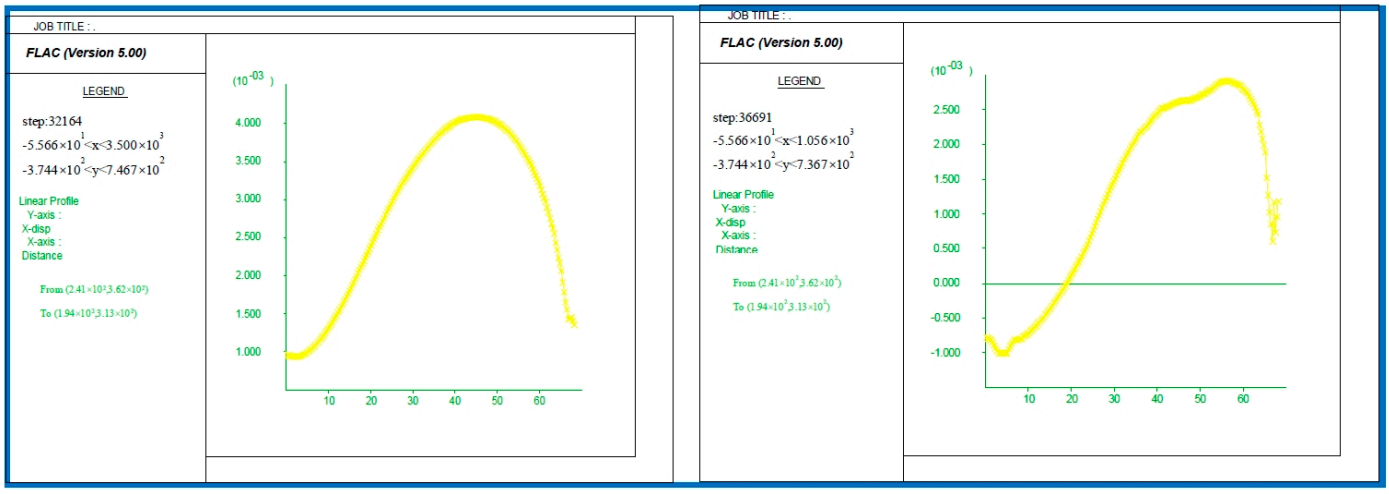

c: Horizontal-displacement distribution curve of slope surface, Unweathered (left), at weathering time of 28 days (right)

Figure 7. Calculated results for slope height of 50 m at angle of 47°.

Regarding the horizontal displacement of the slope surface, a gradual decrease was observed. At the slope's apex, the horizontal displacement was directed positively along the

x-axis. However, as the slope extended downwards, the influence of excavation activities was equal to the displacement, resulting in negative values. This indicated a higher degree of deformation and damage at the slope's base. When comparing slopes with angles of 45° and 47°, an increase in the final slope angle led to an elevation in horizontal stress on the slope surface. To assess the slope's stability, the distribution of plastic zones was analyzed to identify failure-prone areas. It was evident that in the initial excavation stages, prior to weathering of the black shale, there was no discernible presence of plastic zones on the slope surface or within its interior. However, as the weathering process advanced, the extent of plastic zones both on the slope surface and within its depths began to gradually expand. Consequently, the areas susceptible to shear and tensile failures within the slope also increased in scope.

Regarding the impact of weathering effects, it was observed that in the initial stages of weathering, a distinct range of shear and tensile failure areas had already emerged within the slope. At slope angle of 45°, during the early weathering, there was no evidence of plastic failure either on the slope surface or within its interior. However, at the weathering duration of 28 days, extensive plastic zones had developed within the slope, and the slope also exhibited widespread plastic deformation. This underscores that in the later stages of black-shale weathering, the material in its weathered state is susceptible to plastic failure. Comparing the plastic-zone distributions of slopes with angles of 45 and 47, it was evident that as the slope angle increased, the extent of the plastic zone on the slope surface gradually enlarged. The areas of stress, strain, shear failure, and tensile failure within the slope progressively expanded, potentially forming a contiguous zone across the slope surface and interior. Given that the strength of the black shale was significantly reduced after 28 days of weathering, it is advisable to implement appropriate support measures for the exposed slope.

4. Slope Stability Evaluation and Discussion

Utilizing the FLAC finite software (version 5.00), initial findings revealed that when the black-shale slope underwent 28 days of weathering at the slope angle of 47°, the slope's stability was significantly compromised. To further evaluate the potential for slope failure under different scenarios, a slope stability analysis was performed using the limit equilibrium method [40]. This method involves applying static equilibrium conditions to determine the safety factors, which represent the ratio of resisting forces to the driving forces acting on the potential sliding mass. The static equilibrium conditions are applied in both horizontal and vertical directions to the sliding mass. The resisting forces on the sliding surface are calculated based on the shear strength parameters, including cohesion and internal friction angle. When applying the limit equilibrium method to analyze slope stability in open-pit mines, the slope within the mining area is systematically divided into a sequence of vertical slices with uniform width. For each slice, static equilibrium equations are established in both horizontal and vertical directions. By considering any individual slice, the balance of forces in the X- and Y-directions, as well as the moment balance, are calculated. The Swedish arc method is then utilized to derive the expression for calculating the engineering stability coefficient, as outlined in Equation (1). Additionally, when the pore pressure ratio is known, a specific formula is employed to compute the stability coefficient, as detailed in Equation (2). This approach enables a precise assessment of slope stability in open-pit mines, taking into account various factors that influence stability.

$$F = \frac{\sum_{i=1}^{n} [\overline{c} b_i \sec\theta_i + (\gamma h_i - \gamma_w h_{iw}) b_i \cos\theta_i \tan\overline{\varphi}]}{\sum_{i=1}^{n} (W_i \sin\theta_i + Q_i / R)} \quad (1)$$

$$F = \frac{\sum_{i=1}^{n} [\overline{c}b_i \sec\theta_i + (1 - r_u)W_i \cos\theta_i \tan\overline{\varphi}]}{\sum_{i=1}^{n} (W_i \sin\theta_i + Q_i / R)} \quad (2)$$

where C represent effective stress shear strength index of soil cohesion, KPa; φ is the effective stress shear strength index of internal friction angle; α represents the moment arm from the center of gravity of the strip to the center of the sliding arc; R is the radius of the sliding arc, m; Q represents the seismic inertial force (horizontal direction), KN; W is the weight of the strip of soil, KN; θ represents the inclination angle of the sliding surface of the strip; and r_u is the ratio of pore pressure, which is the ratio of the weight of the soil column to the weight of the water column.

The resisting forces on the slope surface are calculated, taking into account the shear strength parameters specific to the black shale as well as the normal stress exerted on each individual slice. The safety factor, a crucial metric, is defined as the ratio between the resisting forces and the driving forces acting on the potential sliding mass. To accurately assess the slope safety factor during various weathering periods, the physical and mechanical parameters are carefully assigned, drawing upon the results of rigorous laboratory tests. Stability calculations are conducted for the slope at different weathering stages, considering two slope angles of 45 and 47, with the aim of exploring the optimal final slope angle under diverse conditions.

Tables 8 and 9 present the calculated safety factors for slopes, considering various combinations of slope angles, heights, and weathering times. For slopes with an angle of 45, it is observed that under identical slope height conditions, the strength of the slope surface rock diminishes gradually as weathering time increases. Consequently, the safety factor of the slope decreases progressively. Additionally, when comparing slopes with the same weathering time, an increase in slope height also contributes to a decrease in the safety factor. Overall, it is evident that the safety factor of the slope decreases with both increasing weathering time and slope height. Furthermore, the safety factors for slopes of 50 m and 90 m are found to comply with the specified requirements. However, for a 120 m slope, as the weathering time gradually increases to 28 days, the safety factor diminishes to 1.085, falling below the minimum safety factor stipulated by the specification.

Table 8. The safety factors under different heights and weathering times at angle of 45°.

Slope Height (m)	0 Days	7 Days	14 Days	21 Days	28 Days
50	1.788	1.773	1.753	1.538	1.130
90	1.598	1.590	1.578	1.567	1.122
120	1.287	1.282	1.276	1.269	1.085

Table 9. The safety factors under different heights and weathering times at angle of 47°.

Slope Height (m)	0 Days	7 Days	14 Days	21 Days	28 Days
50	1.720	1.705	1.683	1.599	1.094
90	1.353	1.346	1.336	1.325	1.050
120	1.230	1.225	1.219	1.231	1.031

For slopes with an angle of 47, it is apparent that an augmentation in the final slope angle leads to a commensurate reduction in the safety factor. After 28 days of weathering, the safety factors for slopes of varying heights are recorded as 1.094, 1.050, and 1.031, all of which are below the minimum safety factor mandated by relevant standards. While these safety factors remain marginally above 1, there is a discernible trend towards instability, particularly for slopes subject to continuous weathering effects [41,42]. This trend is detrimental to slope stability and may signal a potential risk of failure. Consequently, for slopes exceeding 90 m in height, it is prudent to exercise caution when considering a final

slope angle of 47°. If the intended service life surpasses one month, it is generally advisable to avoid such steep slope angles, as they may jeopardize the long-term stability and safety of the slope.

It should be noted that the results obtained through the Fast Lagrangian Analysis of Continua modelling as well as the limit equilibrium methods were based on a reasonable degree of simplification of the models as well as empirical analysis. For example, the boundary conditions and initial stress field were primarily determined by considering the self-weight stress of the rock mass. The obtained numerical results will be also compared with the recorded data in the mine sites in the future. Therefore, the obtained results help us to further understand the effects of weathering on the slope stability, but caution must be taken when using the numerical results as a source of reliable results. The numerical results should be combined with the geological environment conditions, topography, and lithology of the open-pit slope in the mining areas. It is also recommended that further research be conducted in the future and that analysis be undertaken to establish a more explicit relationship between the weathering parameters and the mechanical properties of rock layering at different depths.

5. Conclusions

The impacts of weathering on the stability of open-pit mine slopes were rigorously examined through laboratory tests. The correlation functions between weathering time and mechanical properties were obtained, providing valuable insights into the detrimental effects of weathering on rocks. The finite element method serves as a robust tool to simulate and analyze slope stability under varying weathering conditions. The weathering processes lead to a loosening of the rock structure and a corresponding decrease in its strength and stability. The limit equilibrium methods were used for slope stability analysis, and revealed that an increase in weathering time gradually weakens the slope surface rock, ultimately resulting in a reduction in the slope safety factor. For slopes exceeding 90 m in height, it is advisable to avoid a final slope angle of 47 degrees if the intended service life exceeds one month. This study underscores the crucial importance of considering weathering effects in the design and maintenance of open-pit mine slopes which also help to ensure the long-term stability and safety of the slope structures.

Author Contributions: Conceptualization, W.L. and S.W.; methodology, D.L. and X.K; software, M.Y.; validation, W.L., X.K. and G.S.; formal analysis, M.Y.; resources, W.L., X.K. and G.S.; data curation, W.L., X.K. and G.S.; writing—original draft preparation, S.W. and D.L.; writing—review and editing, S.W. and D.L; project administration, S.W.; funding acquisition, W.L., X.K. and G.S. All authors have read and agreed to the published version of the manuscript.

Funding: This paper is funded by National Natural Science Foundation of China (52474144, 52004196), the Shaanxi Innovation Capability Support Program, the Science and Technology Innovation team (2023CX-TD-12), the Shaanxi Province Department of Education Key Projects of Scientific Research Program (23JS036), and the Ministry of Education, "Chunhui Plan" (HZKY20220534).

Institutional Review Board Statement: Not applicable.

Informed Consent Statement: Not applicable.

Data Availability Statement: The data presented in this study are available on request from the corresponding author.

Conflicts of Interest: Author Wei Liu, Gang Sheng and Xin Kang were employed by the company Shaanxi Provincial Land Engineering Construction Group. The remaining authors declare that the research was conducted in the absence of any commercial or financial relationships that could be construed as a potential conflict of interest.

References

1. Ferrero, A.M. The shear strength of reinforced rock joints. *Int. J. Rock Mech. Min. Sci.* **1995**, *32*, 595–605. [CrossRef]
2. Bieniawski, Z.T. Mechanism of brittle fracture of rock: Part II—Experimental studies. *Int. J. Rock Mech. Min. Sci. Geomech. Abstr.* **1967**, *4*, 407–423. [CrossRef]
3. Hoek, E.; Bieniawski, Z.T. Brittle fracture propagation in rock under compression. *Int. J. Fract. Mech.* **1965**, *1*, 137–155. [CrossRef]
4. Li, Y.C.; Tang, C.A.; Li, D.Q.; Wu, C.Z. A New Shear Strength Criterion of Three-Dimensional Rock Joints. *Rock Mech. Rock Eng.* **2020**, *53*, 1477–1483. [CrossRef]
5. Wu, S.; Ma, X.; Zhang, X.; Chen, J.; Yao, Y.; Li, D. Investigation into hydrogen induced fracture of cable bolts under deep stress corrosion coupling conditions. *Tunn. Undergr. Space Technol.* **2024**, *147*, 105729. [CrossRef]
6. Windsor, C.R. Rock reinforcing systems. *Int. J. Rock Mech. Min. Sci.* **1997**, *34*, 919–951. [CrossRef]
7. Ghobadi, M.H.; Momeni, A.A. Assessment of granitic rocks degradability susceptive to acid solutions in urban area. *Environ. Earth Sci.* **2011**, *64*, 753–760. [CrossRef]
8. Tapponnier, P.; Brace, W.F. Development of stress-induced microcracks in Westerly Granite. *Int. J. Rock Mech. Min. Sci. Geomech. Abstr.* **1976**, *13*, 103–112. [CrossRef]
9. Wu, S.; Hao, W.Q.; Yao, Y.; Li, D.Q. Investigation into durability degradation and fracture of cable bolts through laboratorial tests and hydrogeochemical modelling in underground conditions. *Tunn. Undergr. Space Technol.* **2023**, *138*, 105198. [CrossRef]
10. Gong, B.; Jiang, Y.J.; Chen, L.J. Feasibility investigation of the mechanical behavior of methane hydrate-bearing specimens using the multiple failure method. *J. Nat. Gas Sci. Eng.* **2019**, *69*, 13. [CrossRef]
11. Wang, S.R.; Wu, X.G.; Zhao, Y.H.; Hagan, P.; Cao, C. Evolution Characteristics of Composite Pressure-Arch in Thin Bedrock of Overlying Strata During Shallow Coal Mining. *Int. J. Appl. Mech.* **2019**, *11*, 20. [CrossRef]
12. Gong, B.; Jiang, Y.J.; Yan, P.; Zhang, S.H. Discrete element numerical simulation of mechanical properties of methane hydrate-bearing specimen considering deposit angles. *J. Nat. Gas Sci. Eng.* **2020**, *76*, 17. [CrossRef]
13. Wu, S.S.; Chen, H.H.; Craig, P.; Ramandi, H.L.; Timms, W.; Hagan, P.C.; Crosky, A.; Hebblewhite, B.; Saydam, S. An experimental framework for simulating stress corrosion cracking in cable bolts. *Tunn. Undergr. Space Technol.* **2018**, *76*, 121–132. [CrossRef]
14. Gong, J.; He, M.; Zhang, J.; Liang, W.; Wang, S. Dynamic impact mechanical properties of red sandstone based on digital image correlation method. *Int. J. Min. Reclam. Environ.* **2024**, 1–16. [CrossRef]
15. Gökceoğlu, C.; Ulusay, R.; Sönmez, H. Factors affecting the durability of selected weak and clay-bearing rocks from Turkey, with particular emphasis on the influence of the number of drying and wetting cycles. *Eng. Geol.* **2000**, *57*, 215–237. [CrossRef]
16. Liu, J.Q.; Chen, W.Z.; Liu, T.G.; Yu, J.X.; Dong, J.L.; Nie, W. Effects of Initial Porosity and Water Pressure on Seepage-Erosion Properties of Water Inrush in Completely Weathered Granite. *Geofluids* **2018**, *2018*, 4103645.
17. Wang, S.R.; Xiao, H.G.; Zou, Z.S.; Cao, C.; Wang, Y.H.; Wang, Z.L. Mechanical Performances of Transverse Rib Bar During Pull-Out Test. *Int. J. Appl. Mech.* **2019**, *11*, 15. [CrossRef]
18. Wu, S.S.; Li, J.P.; Guo, J.P.; Shi, G.B.; Gu, Q.H.; Lu, C.W. Stress corrosion cracking fracture mechanism of cold-drawn high-carbon cable bolts. *Mater. Sci. Eng. A-Struct. Mater. Prop. Microstruct. Process.* **2020**, *769*, 10. [CrossRef]
19. Li, Y.C.; Wu, C.Z.; Jang, B.A. Effect of Bedding Plane on the Permeability Evolution of Typical Sedimentary Rocks Under Triaxial Compression. *Rock Mech. Rock Eng.* **2014**, *53*, 5283–5291. [CrossRef]
20. Basu, A.; TCelestino, B.; Bortolucci, A.A. Evaluation of rock mechanical behaviors under uniaxial compression with reference to assessed weathering grades. *Rock Mech. Rock Eng.* **2009**, *42*, 73–93. [CrossRef]
21. Arias, D.; Pando, L.; López-Fernández, C.; Díaz-Díaz, L.M.; Rubio-Ordóñez, Á. Deep weathering of granitic rocks: A case of tunnelling in NW Spain. *Catena* **2016**, *137*, 572–580. [CrossRef]
22. Heidari, M.; Khanlari, G.; Momeni, A.; Jafargholizadeh, H. The relationship between geomechanical properties and weathering indices of granitic rocks, Hamedan, Iran. *Geomech. Geoengin.* **2011**, *6*, 59–68. [CrossRef]
23. Ceryan, S.; Zorlu, K.; Gokceoglu, C.; Temel, A. The use of cation packing index for characterizing the weathering degree of granitic rocks. *Eng. Geol.* **2008**, *98*, 60–74. [CrossRef]
24. Ceryan, S. New weathering indices for evaluating durability and weathering characterization of crystalline rock material: A case study from NE Turkey. *J. Afr. Earth Sci.* **2015**, *103*, 54–64. [CrossRef]
25. Heidari, M.; Momeni, A.A.; Naseri, F. New weathering classifications for granitic rocks based on geomechanical parameters. *Eng. Geol.* **2013**, *166*, 65–73. [CrossRef]
26. Momeni, A.A.; Khanlari, G.R.; Heidari, M.; Sepahi, A.A.; Bazvand, E. New engineering geological weathering classifications for granitoid rocks. *Eng. Geol.* **2015**, *185*, 43–51. [CrossRef]
27. Abad, S.A.N.K.; Tugrul, A.; Gokceoglu, C.; Armaghani, D.J. Characteristics of weathering zones of granitic rocks in Malaysia for geotechnical engineering design. *Eng. Geol.* **2016**, *200*, 94–103. [CrossRef]
28. Wu, S.; Northover, M.; Craig, P.; Canbulat, I.; Hagan, P.C.; Saydam, S. Environmental influence on mesh corrosion in underground coal mines. *Int. J. Min. Reclam. Environ.* **2018**, *32*, 519–535. [CrossRef]
29. Qi, S.; Yue, Z.Q.; Liu, C.; Zhou, Y. Significance of outward dipping strata in argillaceous limestones in the area of the Three Gorges reservoir, China. *Bull. Eng. Geol. Environ.* **2009**, *68*, 195–200. [CrossRef]
30. Wu, S.S.; Ramandi, H.L.; Chen, H.H.; Crosky, A.; Hagan, P.; Saydam, S. Mineralogically influenced stress corrosion cracking of rockbolts and cable bolts in underground mines. *Int. J. Rock Mech. Min. Sci.* **2019**, *119*, 109–116. [CrossRef]

31. Wu, S.; Zhang, X.; Li, J.; Wang, Z. Investigation for influences of seepage on mechanical properties of rocks using acoustic emission technique. *Geofluids* **2020**, *2020*, 6693920. [CrossRef]
32. Momeni, A.; Hashemi, S.S.; Khanlari, G.R.; Heidari, M. The effect of weathering on durability and deformability properties of granitoid rocks. *Bull. Eng. Geol. Environ.* **2017**, *76*, 1037–1049. [CrossRef]
33. Germanovich, L.N.; Salganik, R.L.; Dyskin, A.V.; Lee, K.K. Mechanisms of brittle fracture of rock with pre-existing cracks in compression. *Pure Appl. Geophys.* **1994**, *143*, 117–149. [CrossRef]
34. Wu, S.; Chen, H.; Ramandi, H.L.; Hagan, P.C.; Hebblewhite, B.; Crosky, A.; Saydam, S. Investigation of cable bolts for stress corrosion cracking failure. *Constr. Build. Mater.* **2018**, *187*, 1224–1231. [CrossRef]
35. Erarslan, N.; Williams, D.J. Mixed-Mode Fracturing of Rocks Under Static and Cyclic Loading. *Rock Mech. Rock Eng.* **2013**, *46*, 1035–1052. [CrossRef]
36. Wu, S.; Zhang, Z.R.; Chen, J.H.; Yao, Y.; Li, D.Q. Characterisation of stress corrosion durability and time-dependent performance of cable bolts in underground mine environments. *Eng. Fail. Anal.* **2023**, *150*, 107292. [CrossRef]
37. Zhu, D.; Yu, B.; Wang, D.; Zhang, Y. Fusion of finite element and machine learning methods to predict rock shear strength parameters. *J. Geophys. Eng.* **2024**, *21*, 1183–1193. [CrossRef]
38. Wu, S.; Guo, J.; Shi, G.; Li, J.; Lu, C. Laboratory-Based Investigation into Stress Corrosion Cracking of Cable Bolts. *Materials* **2019**, *12*, 16. [CrossRef]
39. ISRM Society. *Suggested Methods for Determining the Uniaxial Compressive Strength and Deformability of Rock Materials*; International Society for Rock Mechanics: Lisbon, Portugal, 1978; pp. 137–156.
40. Liu, L.-L.; Wang, Y. Quantification of stratigraphic boundary uncertainty from limited boreholes and its effect on slope stability analysis. *Eng. Geol.* **2022**, *306*, 106770. [CrossRef]
41. Rezaei, M.; Seyed, S.Z. Mousavi, Slope stability analysis of an open pit mine with considering the weathering agent: Field, laboratory and numerical studies. *Eng. Geol.* **2024**, *333*, 107503. [CrossRef]
42. Xu, S.; Wang, B.; Wang, D.; Zhang, J. A practical stability/instability chart analysis for slope large deformations using the material point method. *Eng. Geol.* **2024**, *338*, 107611. [CrossRef]